WHISTLER-MODE RESONANCE-CONE EMISSIONS GENERATED BY JUPITER'S MOON IO

by

Lei Xin

A thesis submitted in partial fulfillment of the
requirements of the Master of Science degree in
Physics in the Graduate College of
The University of Iowa

December 2003

Thesis supervisor: Professor Donald A. Gurnett

Graduate College
The University of Iowa
Iowa City, Iowa

CERTIFICATE OF APPROVAL

MASTER'S THESIS

This is to certify that the Master's thesis of

Lei Xin

has been approved by the Examining Committee for the thesis requirement for the Master of Science degree in Physics at the December 2003 graduation.

Thesis committee: __________________________
Thesis supervisor

____
Member

____
Member

ACKNOWLEDGMENTS

Most of all I would like to express my sincere gratitude to my advisor, Professor Donald Gurnett, who provided the initial concept for this project. Without his instructions and patience I could not have been able to complete this thesis.

I would also like to thank Joe Groene and Ann Persoon, who assisted with the plots of the spectrograms and several of the illustrations.

My thanks also go to Kathy Kurth, who helped format this thesis.

Finally, I would like to thank my wife and parents. Without their devotion and sacrifice, I would not have had a chance to study here.

ABSTRACT

During the Galileo spacecraft flyby of Jupiter's moon Io that occurred on Oct. 16, 2001, a well-defined electric field emission was detected by the plasma wave instrument as the spacecraft approached the moon. The spectral characteristics of this emission are very similar to a type of whistler-mode emission called 'auroral hiss' that is commonly observed in the Earth's auroral region. Auroral hiss is believed to be generated by low energy beams of electrons via a coherent Cerenkov radiation mechanism. This thesis gives a detailed analysis of the "auroral hiss" observed near Io.

The electric field spectrum of the auroral hiss emission observed near Io has a sharp high frequency cutoff at the electron cyclotron frequency and a funnel-shaped low frequency cutoff similar to terrestrial auroral hiss. Strong magnetic field perturbations associated with the moon occur right after the onset of the electric noise. To explain the generation mechanism of the auroral hiss observed near Io a brief review of the unipolar inductor theory is given. It is proposed that the observed emission is generated by electron beams in a nearly field-aligned current sheet induced by the interaction of Io with the magnetic field of Jupiter.

The general propagation characteristics of the whistler-mode are discussed. Using the ray-path method the position of the emission source is located assuming that the radiation source has either a point- or sheet-like geometry. The ray

tracing analysis shows that the whistler-mode radiation originates very close to the surface of Io.

TABLE OF CONTENTS

LIST OF TABLES

LIST OF FIGURES

CHAPTER 1

INTRODUCTION

The objective of this thesis is to study an unusual plasma wave emission observed by the Galileo spacecraft during a flyby of Io that occurred on October 16, 2001. The detected emission occurs in the time range from about 0116:30 UT to 0121:30 UT and extends from about 2 to 40 kHz. A frequency-time spectrogram showing the electric field intensity observed during this flyby is shown in Figure 1. The curved low-frequency cutoff of the emission along the left-hand boundary is very similar to that observed for terrestrial auroral hiss, which is a whistler-mode emission frequently observed in the Earth's magnetosphere. The low frequency cutoff of terrestrial auroral hiss usually has a funnel-shaped characteristic similar to Figure 1, but usually with more nearly symmetrical left- and right-hand boundaries. Terrestrial auroral hiss is believed to be produced by low energy (several eV to several keV) beam of auroral electrons via a coherent Cerenkov radiation mechanism.

Ground-based observations of very-low-frequency radio emissions thought to be associated with the aurora were first reported by Martin *et al*. (1960). The first comprehensive spacecraft observations of auroral hiss were made by a very-low-frequency radio receiver on the Injun 3 satellite (Gurnett *et al*., 1964). The Injun 3 satellite also included a magnetic-field aligned photometer that could detect auroral optical emissions. Gurnett (1966) later showed that very-low-frequency radio emissions, now called auroral hiss, were observed on almost every pass over the auroral zone at L values from 6 to 10. From the frequency range of the emissions, which is below the electron plasma frequency and electron cyclotron frequency, and above the proton cyclotron frequency, it was known that the auroral hiss is propagating in the whistler mode. The whistler mode is a mode of propagation first discovered by Storey (1953) to explain a lighting generated phenomena known as whistler. An example of an auroral hiss event observed by the DE 1 spacecraft over Earth's auroral zone is shown in Figure 2. Events of this type typically have a 'funnel-shaped' frequency-time characteristic spectrum. The funnel shape is clearly evident in Figure 2 and is due to whistler-mode propagation near the resonance cone. Gurnett *et al*. (1983) showed that auroral hiss propagates both upward and downward from a spatially localized source at a radial distance between 1.7 and 1.9 R_E. They suggested that the upward propagating auroral hiss detected by DE 1 was produced by an upgoing moving magnetic-field-aligned beam of low-energy electrons via a plasma instability associated with the Laudau resonance at $\upsilon = \omega / k_{//}$. Auroral hiss was also observed near the Io plasma torus at Jupiter by the Voyayer 1 spacecraft (D.A.Gurnett *et al*., 1979). The Jovian auroral hiss also showed a funnel-shaped low frequency cutoff which is very similar to that commonly observed in the Earth's auroral regions. From comparisons with Earth-base observations, it was suggested that the radiation was generated by electrons with energies from about 10 eV to 1 keV and fluxes in the range 10^8 to 10^{10} electrons cm^{-2}.

Next, we discuss evidence of how auroral hiss is produced. The Injun 5 satellite provided the first direct evidence that auroral hiss is generated by intense fluxes, 10^4 to 10^7 electrons cm^{-2}, of low-energy electrons with energies on the order of 100 eV to several keV (D.A.Gurnett *et al*., 1972). But the observed intensities of the auroral hiss indicate that a coherent plasma instability mechanism must be involved in the generation of the hiss, since the intensities are much greater than those expected from an incoherent mechanism such as Cerenkov radiation. Further evidence that auroral hiss is produced by electron beams was provided by a Spacelab 2 (SL-2) electron beam experiment (W.M. Farrell *et al*., 1988). An artificial electron beam was ejected from the space shuttle and the resulting plasma wave emissions were detected by a spacecraft called the Plasma Diagnostics Package (PDP), which was released from the shuttle and flew around the shuttle. A spectrogram showing the plasma wave electric field intensities observed as the PDP flew through the beam is shown in Figure 3. An obvious funnel-shaped emission pattern can be seen centered on the beam. These observations confirmed that the whistler-mode emission from the SL-2 electron beam is propagating upward from the shuttle near the resonance cone, which is a cone of directions relative to the magnetic field along which the index of refraction becomes infinite. The measured wave powers are 10^7 greater than those expected from incoherent Cerenkov radiation, verifying that the radiation is generated by a coherent process.

CHAPTER 2

OBSERVATIONS

In the following we will describe (1) the Galileo plasma wave instruments, and (2) the observations obtained during the October 16, 2001 flyby of Io. The observations include the trajectory of the Galileo spacecraft as it flew by Io, a spectrogram of the electric fields observed in the vicinity of the moon, and a plot of the observed magnetic fields over the same time interval as the spectrogram.

2.1. Description of the Galileo Plasma Wave Instrument

The Galileo plasma wave instrument includes an electric dipole antenna to detect the electric field of plasma waves, and two search coil magnetic antennas to detect magnetic fields. For a description of the instrument see Gurnett *et al.* (1992). Low time resolution spectrums are provided by a step-frequency receiver that covers a frequency range from 5 Hz to 5.6 MHz for electric fields and 5 Hz to 160 kHz for magnetic fields. The frequency resolution in the normal mode of operation is about 10%, and the time resolution for a complete set of electric and magnetic field measurements is 37.33 s. High time resolution spectrums are provided by a wideband receiver, which can provide waveform measurements over bandwidths of 1, 10, and 80 kHz. These measurements can be either transmitted to the ground in real-time, or stored on the spacecraft tape recorder for later transmission to the ground. On the ground the signals are displayed as frequency-time spectrograms. A summary of the principal instrument characteristics is given in Table 1.

2.2. Observations

The Galileo spacecraft, which was placed in the orbit around Jupiter on December 7, 1995, has been carrying out a series of close flybys of the four Galilean satellites. Figure 4 shows the spacecraft trajectory relative to Io from 0050:00 UT to 0210:00 UT on October 16, 2001. This was the sixth close flyby of Io. In this figure, an Io-centered coordinate system is used with the +z axis aligned parallel to Jupiter's rotational axis and the +x axis aligned parallel to the nominal co-rotational plasma flow induced by Jupiter's rotation. The +y axis completes the usual right-handed coordinate system. As can be seen, the spacecraft passed over the south pole of Io with a closest approach at a radial distance of 1.098 R_{Io} at 0123:20 UT.

As described earlier a spectrogram of the electric field intensities obtained from the Galileo plasma instrument in the vicinity of Io is shown in Figure 1. The red color in the spectrum represents the strongest emission while the blue color represents the weakest emission. The dynamic range from dark blue to bright red is 70 dB. The time range is chosen from 0108:00 to 0138:00UT so that the auroral hiss-like emission can be shown clearly. This radiation occurs from 0116:00 to 0121:00 UT and spans a frequency range from about 1 kHz to 40 kHz. The radiation has an asymmetrical funnel-shaped low-frequency cutoff that decreases monotonically from about 40 kHz at 0116:00 UT to about 1 kHz at 0121:00 UT. The electron cyclotron frequency, shown by the white line marked f_{ce} was computed from on-board magnetic field measurements (Kivelson *et al*., 1992) using the equation $f_{ce} = 28\,B$ Hz, where B is in nT. It has a value of about 58 kHz and the proton cyclotron frequency has a value of about 32 Hz. The electron plasma frequency, shown by the white line marked f_{ce}, is also shown in the figure and has a value about 600 kHz during the period of interest. As can be seen, the following inequalities exist among the proton cyclotron frequency f_{ci}, the observed emission frequency f, the electron cyclotron frequency f_{ce}, and the electron plasma frequency f_{pe}:

$$f_{ci} << f << f_{ce} < f_{pe} \,. \tag{2.2.1}$$

For these parameters the only possible mode of propagation in the frequency range of interest is the whistler mode (Stix, 1962). As will be shown shortly these inequalities will allow us to greatly simplify the cold plasma dispersion relation, which will be used later to perform ray-path calculations (see Chapter 3).

Figure 5 gives the plots of the x, y, and z components of the magnetic field in nT for the same time range as in Figure 1. From these plots, it can be seen that all three components of the magnetic field are smooth and slowly varying except in the interval between 0115:00 and 0132:00 UT, which corresponds to the time range when the spacecraft was in the vicinity of Io (comparing with Figure 4). In this interval saw-shaped perturbations are obviously observed in the B_x and B_y plots with perturbations amplitudes of about $\Delta B_x \approx 600$ nT (in a background of -300 nT) and $\Delta B_y \approx 300$ nT (relative to a background of -300 nT). Obvious abrupt changes in magnetic field occurred at about 0121:00 and 0129:00 UT. According to Ampere's law $\nabla \times \vec{B} = \mu_0 \vec{J}$, those changes indicate that the spacecraft crossed two intense current sheets, one near the inner boundary of Io, and the other near the outer boundary of Io. In the region between the two major current sheets, the z-component of magnetic field increased (decreased in magnitude) gradually with small oscillations. After the second current sheet crossing, the B_z field drops down to an equilibrium value of about -1650 nT, which is slightly larger than the field (-1900 nT) that was present during the approach to Io. Comparing with the electric field spectrum, it can be seen that the auroral hiss-like emission occurred when the magnetic perturbation started. The vertex of the funnel-shaped emission occurs almost exactly at the same moment as the first major magnetic field discontinuity. These facts can be explained as follows: when the spacecraft approached the current sheet auroral hiss-like radiation generated by the current was first detected; the radiation was continuously received with strongest wide-spectrum radiation occurring as the spacecraft was right in the current sheet. These data suggest that the auroral hiss is closely associated with the current that cause the discontinuity in the magnetic field. This fact gives further evidence of the presence of a field-aligned current flow connecting Io with Jupiter as proposed by Goldreich and Lynden-Bell (1968). Similar magnetic perturbations of ~5% were also detected earlier by the Voyager 1 magnetometer when the spacecraft crossed Io's magnetic flux tube about 11 R_{Io} below Io (Ness *et al.*, 1979).

CHAPTER 3

THE UNIPOLAR INDUCTOR MODEL

In order to explain the origin of the field-aligned current, which is believed to be responsible for the auroral hiss emission observed during the Io 32 flyby, it is useful to briefly discuss the so called "Unipolar Inductor" model of Io's interaction with the Jovian magnetosphere (Goldreich and Lynden-Bell, 1969). In this chapter, we will discuss (1) Io's influence on Jupiter's decametric emission, and (2) the unipolar inductor model.

It is well known that Jupiter is an intense radio emission source, with radiation extending from decametric wavelengths (Burke, 1955) to kilometric wavelengths (Carr *et al*., 1983). In the process of studying the time variations of these radio emissions, Bigg (1964) found that the emission pattern received on Earth is closely correlated to the geometric position of Io relative to the Earth-Jupiter line. The decametric emission intensity from 1961-1963 is shown in Figure 6 as a function of the departure of Io from superior geocentric conjunction. It can be seen from this figure that the intensity of the emission is closely controlled by the position of Io, with the most intense emissions occurring when Io is about 90 and 240 degrees from superior geocentric conjunction. Superior geocentric conjunction is defined as the moment when Io is located on the far side of the Earth-Jupiter line. The probability of receiving decametric emission on Earth is almost unity at these times. Thus, Bigg showed that Io strongly modulates the intensity of Jupiter's decametric radiation.

The unipolar inductor model is based on two assumptions: first, that the d.c. conductivity of Jupiter's magnetospheric plasma along magnetic field lines is infinite, and zero across the magnetic field lines; and second, that Io is an almost perfect conductor. Goldreich and Lynden-Bell were the first to point out that Io may act as a unipolar inductor, thereby imposing an emf of 7×10^{5} volts across its radial diameter.

This emf drives a current that flows on the surface of the magnetic flux tube connecting Io with Jupiter at a geographical colatitude for the northern foot of $\theta_i = 24^{\text{o}}$. The current starts from the outer face of Io, flows to Jupiter's ionosphere along one-half of the flux tube, then crosses the magnetic field in Jupiter's ionosphere and flows back to Io along the other half of the flux tube to finish the closed current loop (see Figure 7 and Figure 8). The total current is about 10^6 amp and is thought to be carried by keV electrons which are accelerated at Io and Jupiter's ionosphere by a plasma sheath (Gurnett, 1972). The decametric emission is believed to be produced by coherent electron cyclotron radiation from these electrons. The auroral hiss-like emission observed in Figure 1 may be generated by the accelerated electron beam at Io. Confirming evidence of the existence of these filed-aligned currents was provided by magnetic field measurement from the Voyager 1 magnetometer. Figure 9 shows the observed magnetic field perturbation components $\Delta B_x, \Delta B_y$, and the fitting curves for a 2D-dipole and a line current (Ness *et al*., 1980). As can be seen the 2D-dipole source gives a quite good fit to the perturbed field.

The unipolar inductor model has been refined by Neubauer *et al*. (1980). Figure 10 demonstrates the generation of the Alfven wave by a conductor moving perpendicular to uniform magnetic field. It has been shown by Drell (1965) that the current is not really along the magnetic field but rather is carried at an angle to the magnetic field by Alfven waves, the so-called Alfven 'wings' as seen from the satellite frame of reference. The angle between the direction of the Alfven wave propagation and the magnetic field is given by $\theta_A = \tan^{-1} M_A$, where M_A is the Alfven Mach number which is defined by $M_A = u_0 / V_A$ where u_0 is the relative speed between Io and the plasma flow, and $V_A = B / \sqrt{\mu_0 \rho_m}$ is the Alfven speed. Typical parameters for Io are $u_0 \approx 56.8 km/s$, $B \approx 1900 nT$, $V_A \approx 356 km/s$, $M_A \approx 0.16$, and $\theta_A \approx 9.1^\circ$.

CHAPTER 4

THEORY OF WHISTLER-MODE GENERATION AND PROPAGATION

According to Fran Bagenal (1994), the plasma temperature in the Io plasma torus is very low, about 10 eV. Because the low temperature cold plasma theory is expected to be applicable, and is used here to analyze the auroral hiss emission observed by Galileo. In this chapter, the general cold plasma wave dispersion relation is derived from Maxwell's equations and equations of motion for cold plasma (Gurnett and Bhattacharjee, 2001). Then, using two simplifying assumptions, a simple relationship between the resonance cone angle and the whistler-mode wave frequency is obtained. This relationship is used to explain the frequency-time shape of the auroral hiss emission. Finally, the mechanism of the generation and propagation characteristics of the whistler mode is discussed.

4.1. Derivation of the General Dispersion Relation

The "microscopic" and "macroscopic" forms of the Maxwell's equations are given below.

Microscopic	Macroscopic
$\nabla \times \vec{B} = \mu_0 \vec{J} + \varepsilon_0 \mu_0 \dfrac{\partial \vec{E}}{\partial t}$	$\nabla \times \vec{H} = \dfrac{\partial \vec{D}}{\partial t}$
$\nabla \times \vec{E} = -\dfrac{\partial \vec{B}}{\partial t}$	$\nabla \times \vec{E} = -\dfrac{\partial \vec{B}}{\partial t}$

$$(4.1.1)$$

Here, we count all of the charges in the plasma as polarization charges and all the currents are then included in the displacement current $\partial \vec{D} / \partial t$.

Next, we introduce the conductivity tensor $\overleftrightarrow{\sigma}$, defined by $\tilde{\tilde{\vec{J}}} = \overleftrightarrow{\sigma} \bullet \tilde{\tilde{\vec{E}}}$, and the dielectric tensor $\overleftrightarrow{K}$, defined by $\tilde{\tilde{\vec{D}}} = \varepsilon_0 \overleftrightarrow{K} \bullet \tilde{\tilde{\vec{E}}}$. Here the current density is $\tilde{\tilde{\vec{J}}} = \sum_s n_s e_s \tilde{\tilde{\vec{v}}}_s$. When taking the space-time Fourier transformations of the microscopic and macroscopic forms of Ampere's law, we have

$$i\vec{k} \times \tilde{\tilde{\vec{B}}} = \mu_0 \overleftrightarrow{\sigma} \bullet \tilde{\tilde{\vec{E}}} + \varepsilon_0 \mu_0 (-i\omega) \tilde{\tilde{\vec{E}}} \qquad \text{and} \qquad ik \times \tilde{\tilde{\vec{B}}} = \varepsilon_0 \mu_0 (-i\omega) \overleftrightarrow{K} \bullet \tilde{\tilde{\vec{E}}}.$$

Equating the two equations gives the relationship between the dielectric tensor and the conductivity tensor:

$$\overleftrightarrow{K} = \overleftrightarrow{1} - \frac{\overleftrightarrow{\sigma}}{i\varepsilon_0 \omega}.$$

After Fourier transforming, Faraday's and Ampere's laws become

$$i\vec{k} \times \tilde{\tilde{\vec{E}}} = -(-i\omega) \tilde{\tilde{\vec{B}}} \qquad \text{and} \qquad i\vec{k} \times \tilde{\tilde{\vec{B}}} = -\frac{i\omega}{c^2} \overleftrightarrow{K} \bullet \tilde{\tilde{\vec{E}}}.$$

Eliminating $\tilde{\tilde{\vec{B}}}$ between these two equations gives a homogeneous equation for the electric field

$$\vec{k} \times (\vec{k} \times \tilde{\tilde{\vec{E}}}) + \frac{\omega^2}{c^2} \overleftrightarrow{K} \bullet \tilde{\tilde{\vec{E}}} = 0.$$

Using the definition of the index of refraction, $\vec{n} = c\vec{k} / \omega$ the above equation can be expressed in a simpler form

$$\vec{n} \times (\vec{n} \times \tilde{\tilde{\vec{E}}}) + \overleftrightarrow{K} \bullet \tilde{\tilde{\vec{E}}} = 0. \qquad (4.1.2)$$

It can also be written in matrix form as $\vec{\vec{D}} \bullet \tilde{\tilde{\vec{E}}} = 0$. A non-trivial solution for $\tilde{\tilde{\vec{E}}}$ exists if and only if the determinate of the matrix $\vec{\vec{D}}$ is zero, which gives the dispersion relation. The electric field eigenvector associated with each root of the dispersion relation can be obtained from the homogeneous equations (4.1.2), and the corresponding magnetic field eigenvector can be obtained from Faraday's law $\tilde{\tilde{\vec{B}}} = (\vec{k}/\omega) \times \tilde{\tilde{\vec{E}}}$ or $c\tilde{\tilde{\vec{B}}} = \vec{n} \times \tilde{\tilde{\vec{E}}}$.

4.2 Waves in Cold Uniform Magnetized Plasma

We consider the case of cold plasma with an externally imposed static uniform magnetic field $\vec{B}_0 = B_0 \hat{z}$. The linearized equation of motion for a single particle is then

$$m_s \frac{d\vec{v}_s}{dt} = e_s \left[\vec{E}_1 + \vec{v}_1 \times \vec{B}_0\right]. \tag{4.2.1}$$

After Fourier transforming, the above equation becomes

$$\begin{aligned} -i\omega m_s \tilde{v}_{sx} &= e_s \left[\tilde{\tilde{E}}_x + \tilde{v}_{sy} B_0\right] \\ -i\omega m_s \tilde{v}_{sy} &= e_s \left[\tilde{\tilde{E}}_y - \tilde{v}_{sx} B_0\right] \\ -i\omega m_s \tilde{v}_{sz} &= e_s \tilde{\tilde{E}}_z . \end{aligned} \tag{4.2.2}$$

By introducing the cyclotron frequency, $\omega_{cs} = e_s B_0 / m_s$ the above equations can be written in matrix form as

$$\begin{bmatrix} -i\omega & -\omega_{cs} & 0 \\ \omega_{cs} & -i\omega & 0 \\ 0 & 0 & -i\omega \end{bmatrix} \begin{bmatrix} \tilde{v}_{sx} \\ \tilde{v}_{sy} \\ \tilde{v}_{sz} \end{bmatrix} = \frac{e_s}{m_s} \begin{bmatrix} \tilde{\tilde{E}}_x \\ \tilde{\tilde{E}}_y \\ \tilde{\tilde{E}}_z \end{bmatrix}. \tag{4.2.3}$$

Solving for $\tilde{v}_{sx}$, $\tilde{v}_{sy}$ and $\tilde{v}_{sz}$ gives

$$\begin{bmatrix} \tilde{v}_{sx} \\ \tilde{v}_{sy} \\ \tilde{v}_{sz} \end{bmatrix} = \frac{e_s}{m_s} \begin{bmatrix} \frac{-i\omega}{\omega_{cs}^2 - \omega^2} & \frac{\omega_{cs}}{\omega_{cs}^2 - \omega^2} & 0 \\ \frac{-\omega_{cs}}{\omega_{cs}^2 - \omega^2} & \frac{-i\omega}{\omega_{cs}^2 - \omega^2} & 0 \\ 0 & 0 & \frac{i}{\omega} \end{bmatrix} \begin{bmatrix} \tilde{E}_x \\ \tilde{E}_y \\ \tilde{E}_z \end{bmatrix}. \tag{4.2.4}$$

The current $\tilde{\vec{J}} = \sum_s n_s e_s \tilde{\vec{v}}_s$ becomes

$$\begin{pmatrix} \tilde{J}_x \\ \tilde{J}_y \\ \tilde{J}_z \end{pmatrix} = \sum_s \frac{n_{s0} e_s^2}{m_s} \begin{pmatrix} \frac{-i\omega}{\omega_{cs}^2 - \omega^2} & \frac{\omega_{cs}}{\omega_{cs}^2 - \omega^2} & 0 \\ \frac{-\omega_{cs}}{\omega_{cs}^2 - \omega^2} & \frac{-i\omega}{\omega_{cs}^2 - \omega^2} & 0 \\ 0 & 0 & \frac{i}{\omega} \end{pmatrix} \begin{pmatrix} \tilde{E}_x \\ \tilde{E}_y \\ \tilde{E}_z \end{pmatrix}. \tag{4.2.5}$$

Comparing with $\tilde{\vec{J}} = \overleftrightarrow{\sigma} \bullet \tilde{\vec{E}}$, we have conductivity tensor

$$\overleftrightarrow{\sigma} = \sum_s \frac{n_{s0} e_s^2}{m_s} \begin{pmatrix} \frac{-i\omega}{\omega_{cs}^2 - \omega^2} & \frac{\omega_{cs}}{\omega_{cs}^2 - \omega^2} & 0 \\ \frac{-\omega_{cs}}{\omega_{cs}^2 - \omega^2} & \frac{-i\omega}{\omega_{cs}^2 - \omega^2} & 0 \\ 0 & 0 & \frac{i}{\omega} \end{pmatrix}. \tag{4.2.6}$$

Finally, the dielectric tensor has form

$$\overleftrightarrow{K} = \begin{bmatrix} S & -iD & 0 \\ iD & S & 0 \\ 0 & 0 & P \end{bmatrix}, \tag{4.2.7}$$

where

$$S = 1 - \sum_s \frac{\omega_{ps}^2}{\omega^2 - \omega_{cs}^2}, \qquad D = \sum_s \frac{\omega_{cs}\omega_{ps}^2}{\omega(\omega^2 - \omega_{cs}^2)},$$

$$P = 1 - \sum_s \frac{\omega_{ps}^2}{\omega^2} \qquad \text{and}$$

the plasma frequency is given by $\omega_{ps}^2 = \dfrac{n_{s0}e_s^2}{\varepsilon_0 m_s}$.

Following Stix [1992], the terms S and D can be decomposed into a sum and difference using the relation

$$S = \frac{1}{2}(R + L) \qquad \text{and} \qquad D = \frac{1}{2}(R - L),$$

where R and L are defined by

$$R = 1 - \sum_s \frac{\omega_{ps}^2}{\omega(\omega + \omega_{cs})} \qquad \text{and} \qquad L = 1 - \sum_s \frac{\omega_{ps}^2}{\omega(\omega - \omega_{cs})}$$

Without loss of generality, let the index of refraction vector be $\vec{n} = (n\sin\theta, 0, n\cos\theta)$. Then the homogeneous equation (4.1.2) can be written as

$$\begin{bmatrix} S - n^2\cos^2\theta & -iD & n^2\sin\theta\cos\theta \\ iD & S - n^2 & 0 \\ n^2\sin\theta\cos\theta & 0 & P - n^2\sin^2\theta \end{bmatrix} \begin{bmatrix} \tilde{E}_x \\ \tilde{E}_y \\ \tilde{E}_z \end{bmatrix} = 0. \tag{4.2.8}$$

This equation has nontrivial solution if and only if the determinant of the matrix is zero, which gives the dispersion relation

$$D(\vec{n}, \omega) = n^2\sin\theta\cos\theta[-(S - n^2)n^2\sin\theta\cos\theta] +$$
$$[P - n^2\sin^2\theta][(S - n^2)(S - n^2\cos^2\theta) - D^2] = 0$$

or

$$D(\vec{n},\omega) = An^4 - Bn^2 + RLP = 0\,. \tag{4.2.9}$$

where $A = S\sin^2\theta + P\cos^2\theta$ and $B = RL\sin^2\theta + PS(1+\cos^2\theta)$. This equation can solve as:

$$n^2 = \frac{B \pm F}{2A} \tag{4.2.10}$$

where $F^2 = (RL - PS)^2 \sin^4\theta + 4P^2D^2\cos^2\theta$.

If we use $1 = \sin^2\theta + \cos^2\theta$ and sort out the $\sin^2\theta$ and $\cos^2\theta$ terms in the dispersion relation (4.2.9), we can get the "tangent" form

$$\tan^2\theta = \frac{-P(n^2 - R)(n^2 - L)}{(Sn^2 - RL)(n^2 - P)}\quad , \tag{4.2.11}$$

which is sometimes useful. To obtain a tractable equation for the index of refraction of the whistler mode, we make two assumptions. First, we ignore the ions terms since they response much more slowly than the electron in the frequency of interest due to their heavy masses. Second, we assume that both the wave frequency and the electron cyclotron frequency are both much less than the electron plasma frequency, i.e., $\omega^2 << \omega_p^2$ and $\omega_c^2 << \omega_p^2$. These conditions are satisfied in our case since, first, the auroral hiss emission region is well below the electron cyclotron frequency (see Figure 1) i.e., $f < f_c$ and, second, the plasma frequency $f_p \approx 590$ kHz (from the spectrum data) is about ten times greater than $f_c \approx 58$ kHz.

With these assumptions, the expressions for R, L, D, S, and P can be approximated as follows:

$$R \approx \frac{-\omega_p^2}{\omega(\omega-\omega_c)} \;, \qquad L \approx \frac{-\omega_p^2}{\omega(\omega+\omega_c)}$$

$$S \approx \frac{-\omega_p^2}{\omega^2-\omega_c^2} \;, \qquad D \approx \frac{-\omega_p^2\omega_c}{\omega(\omega^2-\omega_c^2)}$$

$$P \approx -\frac{\omega_p^2}{\omega^2} .$$

Since it is easily verified that $RL = PS$, the quantities A, B and F in equation (4.2.10) simplify to the following

$$A \approx \frac{\omega_p^2(\omega^2-\omega_c^2\cos^2\theta)}{\omega^2(\omega^2-\omega_c^2)} \;, \qquad B \approx \frac{2\omega_p^4}{\omega^2(\omega^2-\omega_c^2)}$$

$$F \approx 2\frac{\omega_p^4\omega_c}{\omega^3(\omega^2-\omega_c^2)}\cos\theta .$$

Substituting those expressions into equation (4.2.10), the index of refraction is given by

$$n^2 = \frac{\omega_p^2}{\omega(\omega_c\cos\theta-\omega)} . \qquad (4.2.12)$$

Three polar plots of the surface of the index of refraction surface $n(\theta)$ at frequencies f_1, f_2 and f_3 are shown in Figure 11. The resonance cone is defined as the locus of points where the index of refraction goes to infinity. The corresponding wave normal angle is called the resonance cone angle, which in this case is given by $\cos\theta_{\mathrm{Res}} = \omega/\omega_c$. Since the group velocity of wave propagation is perpendicular to the index of refraction surface, then the angel ψ, between the direction of the group velocity and the magnetic field is given by $\psi = \pi/2 - \theta_{\mathrm{Res}}$. It follows then that the group velocity direction, which is the direction of energy flow is given by

$$\sin\psi = f / f_c . \tag{4.2.13}$$

It is obvious that the higher frequencies have larger angels of propagation. Figure 12 shows a simple point source near Io. When observer approaches the radiation source from left, the highest radiation frequency f_3 is receivedfirst, then the smaller frequencies f_2 and f_1 will be detected.

4.3. Origin of the Funnel Shape

In order to explain the distinguishing funnel-shaped cutoff characteristic of the auroral hiss, we consider a simple two-dimensional model. Two assumptions are made to simplify the model: first, that the magnetic field is uniform everywhere and is perpendicular to the trajectory of the spacecraft, and second, that the radiation source is a point source. To carry out a simplified analysis, we introduce a coordinate x, which is the perpendicular distance from the spacecraft to the magnetic field line through the source and a distance h, which is the height of the spacecraft above the source (see Figure 13). Then a simple geometry shows

$$\tan\psi = \frac{x}{h} . \tag{4.3.1}$$

From (4.2.13) we derive

$$\tan\psi = \frac{f}{\sqrt{f_c^2 - f^2}} . \tag{4.3.2}$$

Equating those equations gives the low-frequency cutoff

$$f^2 = f_c^2 - \frac{h^2}{x^2 + h^2} f_c^2 . \tag{4.3.3}$$

This equation is a hyperbola with an upper frequency limit f_c. Figure 14 is a frequency-time spectrum of radiation from such a source that demonstrates the funnel-shaped frequency-time characteristics. The dotted region is filled by radiation if the radiation source is a line along the magnetic field instead of a single point source. The received radiation is just the superposition of various point sources. Also seen from Figure 14, the two branches of funnel-shaped low frequency cutoff are symmetric about the radiation source.

CHAPTER 5

MODEL CALCULATION

The left-hand side of the auroral hiss emission observed by Galileo (see Figure 1) has a frequency-time shape very similar to the funnel shape predicted by the simple model shown in Figure 14. This close similarity indicates that we can use the whistler-mode propagation near resonance cone to locate the emission source. In the following, we will locate the possible source of radiation by finding the best fit to the funnel-shaped low frequency cutoff using a more exact geometry model that takes into account the actually spacecraft trajectory. Initially we will assume the radiation source is a simple point source. Then later we will investigate the possibility that the radiation source is a sheet source aligned along magnetic field lines that are tangent to the surface of Io.

5.1. A Simple Model: Point Source Emission

Recall that under the assumptions $f^2 << f_p^2$ and $f_c^2 << f_p^2$ we have $\sin\psi = f / f_c$, where ψ is the angle between the limiting ray path direction and the magnetic field, f is the cutoff frequency, and f_c is the electron cyclotron frequency.

To compare the theoretical model with the observations, we first calculate the time dependent of the cutoff frequency from the simple geometric relation of the Galileo trajectory. Figure 15 shows the geometric relation for computing ψ, the angle between the limiting ray path and the magnetic field through the emission source. $R(x, y, z)$ is an arbitrary point on the trajectory of Galileo; $R(x_s, y_s, z_s)$ represents the position of the emission source; $R_0(x_0, y_0, z_0)$ is a point when the spacecraft is on the magnetic line through the source. Obviously, R_0 and R_s are two adjustable points. Recall that R_0 is a point where the lowest frequency of the emission of the cutoff boundary is received, by inspecting the spectrum in Figure 1, we find that the low frequency apex of the emission occurs at about 0120:00 UT, which corresponds to spacecraft coordinates $(x_0, y_0, z_0) = (-0.893, 0.24, -1.019)$. We fix the point R_0. Next the height of the source $h = |\vec{R}_0 - \vec{R}_s|$ is adjusted until a best-fit cutoff boundary is found. In the following we will show the detail of the calculation.

If the height of the emission source h is given, then the coordinates of the source $R(x_s, y_s, z_s)$ can be calculated by simple geometry relations:

$$\frac{x_0 - x_s}{B_x} = \frac{y_0 - y_s}{B_y} = \frac{z_0 - z_s}{B_z} = \frac{h}{B}.$$

So, we have

$$x_s = x_0 - \frac{h}{B} B_x, \quad y_s = y_0 - \frac{h}{B} B_y \text{ and } z_s = z_0 - \frac{h}{B} B_z.$$

Then the calculation of the cutoff frequency f is straightforward. For each point in the range 0115:00 UT to 0120:00 UT (where the auroral hiss-like radiation occurs) on the trajectory $R(x, y, z)$, calculate the angle ψ between $\vec{R} - \vec{R}_s$ (the limiting ray path) and $\vec{R}_0 - \vec{R}_s$ (the magnetic field line):

$$\cos\psi = \frac{(\vec{R} - \vec{R}_s) \bullet (\vec{R}_0 - \vec{R}_s)}{\left|\vec{R} - \vec{R}_s\right| \left|\vec{R}_0 - \vec{R}_s\right|}$$

$$= \frac{(x - x_s)(x_0 - x_s) + (y - y_s)(y_0 - y_s) + (z - z_s)(z_0 - z_s)}{\sqrt{(x - x_s)^2 + (y - y_s)^2 + (z - z_s)^2}\sqrt{(x_0 - x_s)^2 + (y_0 - y_s)^2 + (z_0 - z_s)^2}}$$

$$\sin\psi = \sqrt{1 - (\cos\psi)^2}.$$

Recall that the cutoff frequency is given by

$$f = f_c \sin\psi \, .$$

Using the above equation we get the time dependent of the cutoff frequency $f = f(t)$. Figure 16 shows the results for three different values of h. The solid points in Figure 16 are sampled from the cutoff boundary of the spectrum Figure 1. From Figure 16 we can see that the position of the source is located roughly between $h = 0.65$ and $h = 1.15$, here h is in the unit of the radius of Io. The wide range of h indicates that the source doesn't have a sharp defined low-altitude boundary. That is reasonable since the emission spectrum in Figure 1 doesn't have a sharply defined frequency-time boundary. The best fit to the cutoff frequency data gives $h = 0.9$, which corresponds to the source position at coordinates $R_s(x_s, y_s, z_s) = (-1.035, 0.469, -0.16)$. The small value of z_s indicates that the source lies near the equator of Io, roughly in the region where Jupiter's magnetic field is tangent to the surface of Io. The best-fitting cutoff curve is also drawn in the spectrum for comparison as Figure 17 shows.

5.2. Calculation Based on a Sheet Source

Since the frequency-time spectrum of the radiation is filled in instead of being a sharp line, it is likely that the source of the emission is either a line or a sheet source. Applying the unipolar inductor model, we consider the possibility that the source is a cylindrical current sheet (see Figure 18). We choose the axis of the cylinder in the direction of the magnetic field line at R_0 through the center of the Io with radius $r = \sqrt{x_s^2 + y_s^2 + z_s^2}$ =1.15>1 (which is reasonable since the current source is most likely produced in the ionosphere of the Io). Since we have no information of the magnetic field out of the trajectory, we simply assume that the local current sources responsible for the radiation are also along B_0 at R_0. Also for simplicity, we draw a plane p with its normal along z direction through point R_s (the point source giving good fit as previous calculation shows.). The intersection between the plane p and the cylindrical current sheet makes a curve C. For every individual point on the trajectory $R(x, y, z)$ (see Figure 18), we draw the normal of current cylinder $R_0^{'}R$. (Note: $R_0^{'}$ lies on the surface of the cylinder). Line $R_s^{'}R_0^{'}$ is parallel to B_0 and intersects with curve C at point $R_s^{'}$ which we look it as the point source responsible for the cutoff frequency at $R(x, y, z)$. The coordinates of $R_0^{'}(x_0^{'}, y_0^{'}, z_0^{'})$ and $R_s^{'}(x_s^{'}, y_s^{'}, z_s^{'})$ can be calculated as follows:

Define the unit vector of B_0 as n_B= (a, b, c) = (0.158,-0.254,-0.954), then the coordinates of point $R_1(x_1, y_1, z_1)$ satisfy

$$\begin{aligned}
&\frac{x_1}{a} = \frac{y_1}{b} = \frac{z_1}{c} = k_1 \\
&x_1 = ak_1 \\
&y_1 = bk_1 \\
&z_1 = ck_{1.}
\end{aligned} \tag{5.2.1}$$

$$R_1R \bullet n_B = 0 \Rightarrow (x - x_1)a + (y - y_1)b + (z - z_1)c = 0.$$

So, we have $k_1 = \dfrac{ax + by + cz}{a^2 + b^2 + c^2}$. Substitute k_1 into (5.2.1), we have $R_1(x_1, y_1, z_1)$.

The equation of line $R_1R_0^{'}R$ is

$$\begin{aligned}
&\frac{x_0^{'} - x_1}{x - x_1} = \frac{y_0^{'} - y_1}{y - y_1} = \frac{z_0^{'} - z_1}{z - z_1} = k_2 \Rightarrow \\
&x_0^{'} = k_2(x - x_1) + x_1 \\
&y_0^{'} = k_2(y - y_1) + y_1 \\
&z_0^{'} = k_2(z - z_1) + z_1
\end{aligned} \tag{5.2.2}$$

In fact, $k_2 = \dfrac{r}{\sqrt{(x - x_1)^2 + (y - y_1)^2 + (z - z_1)^2}}$. Substitute k_2 into (5.2.2), we get the coordinates of $R_0^{'}(x_0^{'}, y_0^{'}, z_0^{'})$.

To find $R_s^{'}(x_s^{'}, y_s^{'}, z_s^{'})$, note that $\vec{R}_0^{'} - \vec{R}_s^{'}$ is parallel to $\vec{B}_0$ so

$$
\begin{aligned}
&\frac{x_s^{'} - x_0^{'}}{a} = \frac{y_s^{'} - y_0^{'}}{b} = \frac{z_s^{'} - z_0^{'}}{c} = k_3 \Rightarrow \\
&x_s^{'} = ak_3 + x_0^{'} \\
&y_s^{'} = bk_3 + y_0^{'} \\
&z_s^{'} = ck_3 + z_0^{'}
\end{aligned}
\tag{5.2.3}
$$

Recall $z_s^{'} = z_s \Rightarrow k_3 = \frac{z_s - z_0^{'}}{c}$. Plug k_3 into (5.2.3), we can have the coordinates of $R_s^{'}(x_s^{'}, y_s^{'}, z_s^{'})$. Once we have the coordinates of $R_0^{'}(x_0^{'}, y_0^{'}, z_0^{'})$ and $R_s^{'}(x_s^{'}, y_s^{'}, z_s^{'})$, we can calculate the angle ψ between $\vec{R} - \vec{R}_s^{'}$ (the limiting ray paths) and $\vec{R}_0^{'} - \vec{R}_s^{'}$ (The magnetic field line). It is given by

$$
\cos\psi = \frac{(\vec{R} - \vec{R}_s^{'}) \bullet (\vec{R}_0^{'} - \vec{R}_s^{'})}{\left|\vec{R} - \vec{R}_s^{'}\right|\left|\vec{R}_0^{'} - \vec{R}_s^{'}\right|} = \frac{(x - x_s^{'})(x_0^{'} - x_s^{'}) + (x - x_s^{'})(y_0^{'} - y_s^{'}) + (z - z_s^{'})(z_0^{'} - z_s^{'})}{\sqrt{(x - x_s^{'})^2 + (x - x_s^{'})^2 + (z - z_s^{'})^2}\sqrt{(x_0^{'} - x_s^{'})^2 + (y_0^{'} - y_s^{'})^2 + (z_0^{'} - z_s^{'})^2}}
$$

Finally, the time dependent cutoff frequency is given by

$$
f = f_c \sin\psi .
$$

Figure 19 shows the cutoff fitting curve calculated by assuming a sheet emission source. The solid circles are sampled from the cutoff boundary of the spectrum data of the auroral-hiss emission, while the solid line represents the fitting curve calculated above. As can be seen, the ray tracing fit to the observed spectrum is quite good. That indicates that the emission source responsible for the auroral-hiss emission could be a sheet source. The good fit also indicates that the trajectory of the spacecraft is nearly perpendicular to the cylindrical current sheet.

As can be seen from Figure 16 and Figure 19, the funnel-shaped low frequency cutoff calculated by assuming the emission source is either a point source or a cylindrical sheet source fit quite good to the observed auroral-hiss spectrum, which provides strong verification that the whistler-mode emission is propagating at angles very close to the resonance cone, as has been assumed. The emission source has a poorly defined low-altitude boundary since the funnel shaped cutoff boundary of the emission spectrum is not clearly defined.

CHAPTER 6

SUMMARY AND INTERPRETATION

Broadband auroral hiss-like emissions have been observed by the Galileo spacecraft near Jupiter’s moon Io. The frequency range of the emission occurs well below the local electron cyclotron frequency and the local electron plasma frequency, and above the proton cyclotron frequency. The frequency range indicates that the emissions are propagating in whistler mode. Seen from the electric field spectrogram, the emission has a funnel-shaped low frequency cutoff characteristic which is very similar to the terrestrial auroral hiss commonly observed in the Earth’s auroral region. The close association of the central axis of the funnel with the onset of the perturbation of the magnetic field caused by Io indicates that the emission is probably generated by a current sheet originating from Io. This current sheet is most likely produced by the unipolar inductor interaction of Io with the Jovian magnetic field. Since auroral hiss is known to be produced by electron beams, these observations indicate the existence of a downward electron beam accelerated near Io. That means that the real direction of the current is upward pointing toward Io. The direction of the current agrees well with that proposed by the unipolar inductor model.

The difference of the emissions from most earth observed auroral hiss is that it doesn’t have an obvious funnel-shaped low frequency cutoff on its right-hand branch. Since no detailed information is available on the plasma parameters in the inner and outer regions of the flux tube, one possible explanation of the asymmetry of the emission is that the plasma inside the flux tube is hot compared to that outside the flux tube and the emission is strongly absorbed by the hot plasma. The same emission is also observed at the exit of the flux tube which occurs at about 0130:00. Those emissions have an upper frequency cutoff at about 15 kHz which is about three times lower than that of the emissions observed as the spacecraft approaches the flux tube. That may indicate that the current carriers on the outer region of the flux tube have lower kinetic energy than those on the inner region of the flux tube.

Assuming that the emission is propagating in the whistler mode near the resonance cone, the low-altitude boundary of the current source generating the emission is derived by ray tracing calculations which give best fit to the funnel-shaped low frequency cutoff. A series of ray tracing computations have been performed by assuming a point and cylindrical sheet emission sources. It is found that the low-altitude boundary of the current source lies at near the equatorial plane of Io with coordinates $(-1.035, 0.469, -0.16)$, which corresponds to a height of about 270 km from the surface of Io. From the electron density profile of the ionosphere of Io given by Kliore *et al*. (1974), we can see that the current source well lies in the ionosphere of Io with a local electron density about 3×10^4 electrons per cubic centimeter. It is also shown that the source has a rough low-altitude boundary between 0.65-1.15 R_{Io} below the spacecraft along the local magnetic field line. The generation mechanism of this emission is commonly believed by a coherent Cerenkov radiation. The auroral-hiss emission observed by Galileo is likely generated by downstream electron beams accelerated in the ionosphere of Io. One possible acceleration mechanism is the plasma sheath around Io as proposed by Gurnett (1972).

TABLE 1

PLASMAWAVE INSTRUMENT CHARACTERISTICS

Parameter	Characteristic	
Frequency range, electric	5.62 Hz to 5.65 MHz	
Frequency range, magnetic	5.62 Hz to 160 kHz	
Frequency resolution	(Low freq.) 5.62 Hz to 31.1 Hz, $\Delta f / f \cong 67\%$ (Med. freq.) 40 Hz to 160 kHz, $\Delta f / f \cong 8\%$ (High freq.) 100 kHz to 5.65 MHz, $\Delta f / f = 10\%$	
Time resolution	(Low freq.) 5.62 Hz to 31.1 Hz, $\Delta t \cong 2.67\,s$ (Med. freq.) 40 Hz to 160 kHz, $\Delta t \cong 18.67\,s$ (High freq.) 100 kHz to 5.65 MHz, $\Delta t = 18.67s$	
Sensitivity, electric	$E\sqrt{\Delta f} \cong$ 15 nV m^{-1} $Hz^{-1/2}$ at ~10 kHz	
Sensitivity, magnetic	$B\sqrt{\Delta f} \cong 50\ \mu y$ $Hz^{-1/2}$ at ~ 100 Hz decreasing to $\cong 3\ \mu y$ $Hz^{-1/2}$ at ~ 20 Hz	
Dynamic range	5.62 Hz to 31.1 Hz, 100 dB 40 Hz to 5.65 MHz, 100 dB	
Wideband waveform modes	Mode 1, 50 Hz to 10 kHz Mode 2, 50 Hz to 80 kHz Mode 3, 5 Hz to 1 kHz	
Waveform resolution	Mode 1, 4-bits, 25 200 samples s^{-1} Mode 2, 4-bits, 201 600 samples s^{-1} Mode 3, 4-bits, 3150 samples s^{-1}	
Mass	Main electronics box Search coil Electric antenna Total	3.94 kg 1.52 <u>1.68</u> 7.14 kg
Power	6.80 W, heater power 3.0 W	

Figure 1. Semi-log plot of the time-frequency spectrum of the electric field for the time series from 0108:20 UT to 0138:20 UT, October 16, 2001.

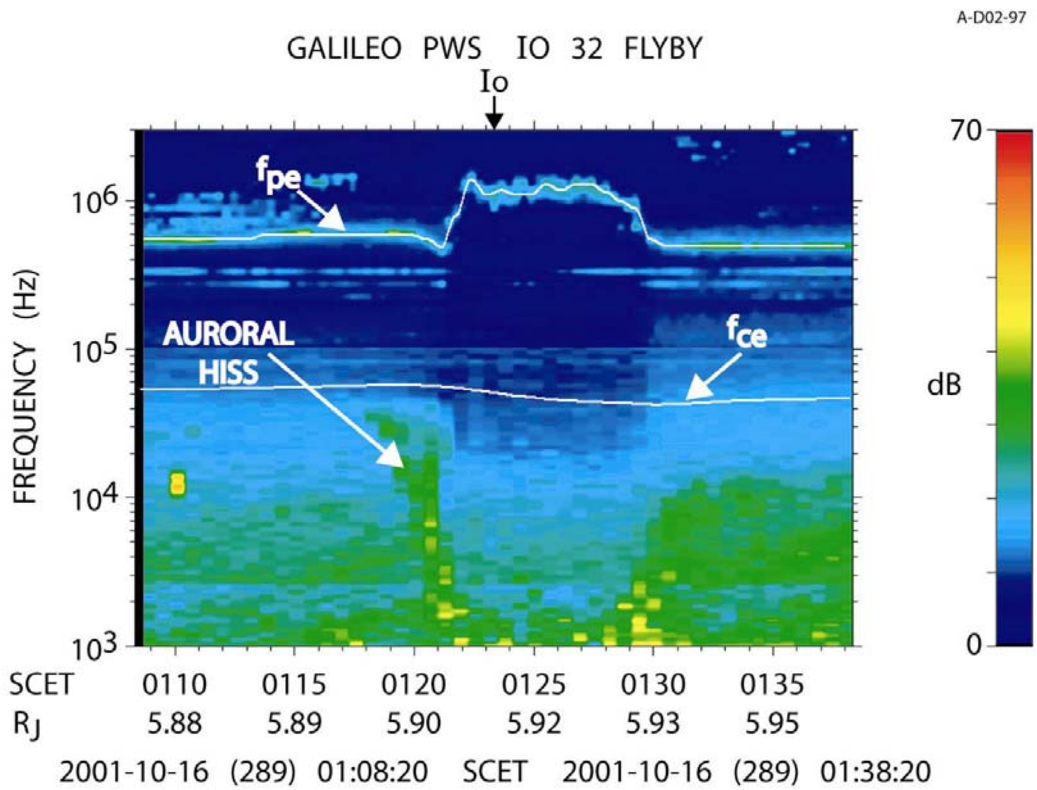

A-D02-97
GALILEO PWS IO 32 FLYBY
Io
FREQUENCY (Hz)
10^6
10^5
10^4
10^3
f_pe
AURORAL HISS
f_ce
70
dB
0
SCET 0110 0115 0120 0125 0130 0135
R_J 5.88 5.89 5.90 5.92 5.93 5.95
2001-10-16 (289) 01:08:20 SCET 2001-10-16 (289) 01:38:20

Figure 2. Auroral hiss observed by DE 1 spacecraft. (Reprinted from D.A. Gurnett (1983).)

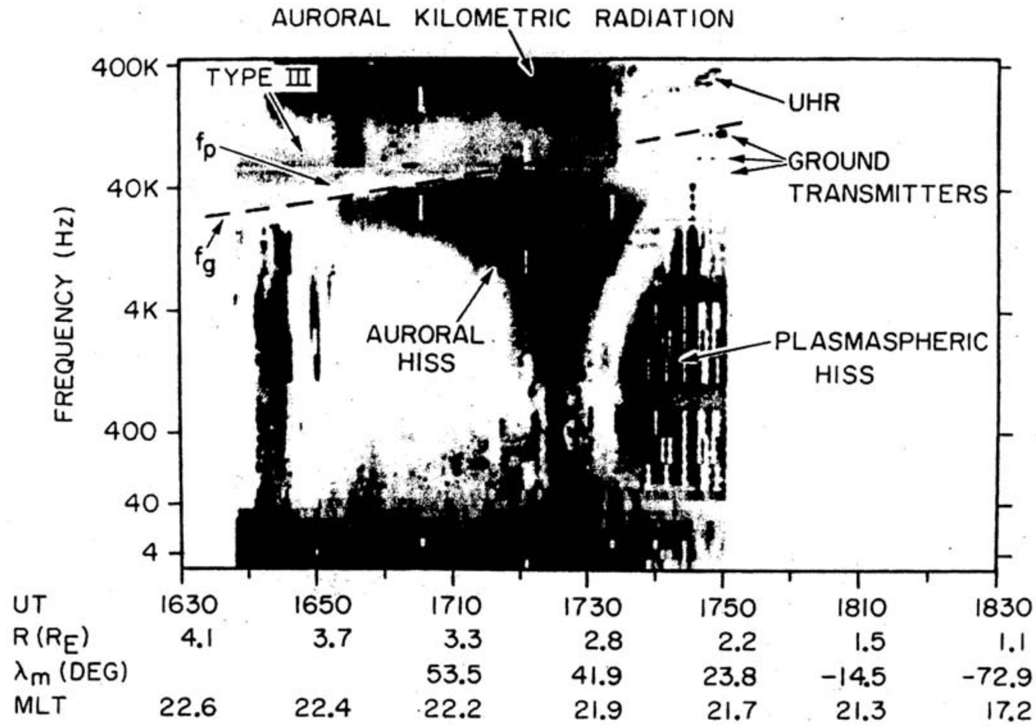

ELECTRIC FIELD, DE-1, OCTOBER 15, DAY 288, 1981

Figure 3. A frequency-versus-time spectrogram from the PDP plasma wave instrument. The funnel-shaped structure that extends from the electron cyclotron frequency to about 30 kHz is whistler-mode radiation from the man-made electron beam. (Reprinted from Farrell (1988).)

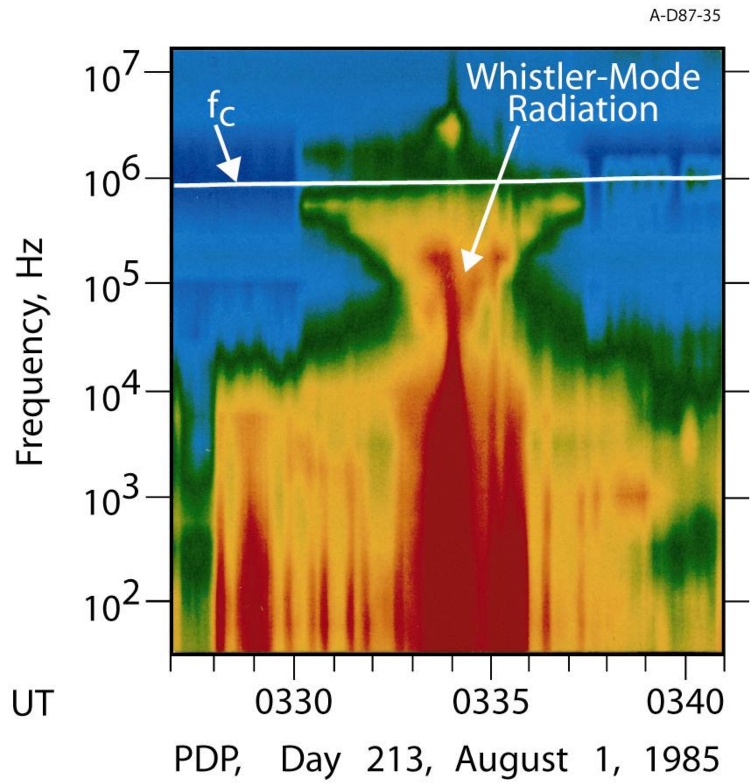
A-D87-35
Whistler-Mode
Radiation
f_c
10^7
10^6
10^5
10^4
10^3
10^2
Frequency, Hz
UT
0330
0335
0340
PDP, Day 213, August 1, 1985

Figure 4. The trajectory of Galileo during the Io 32 flyby.

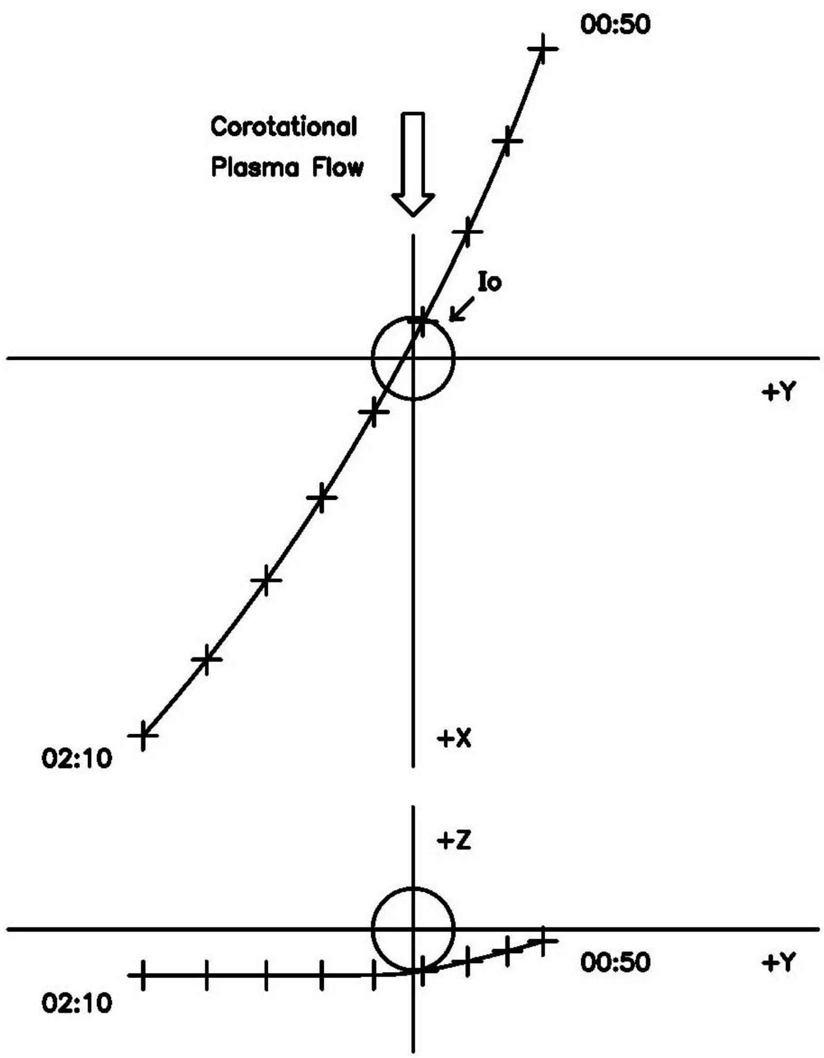
00:50
Corotational
Plasma Flow
Io
+Y
+X
02:10
+Z
00:50
+Y
02:10

Figure 5. Magnetic field components measured by the Galileo magnetometer on October 16, 2001, plotted versus spacecraft event time in UT.

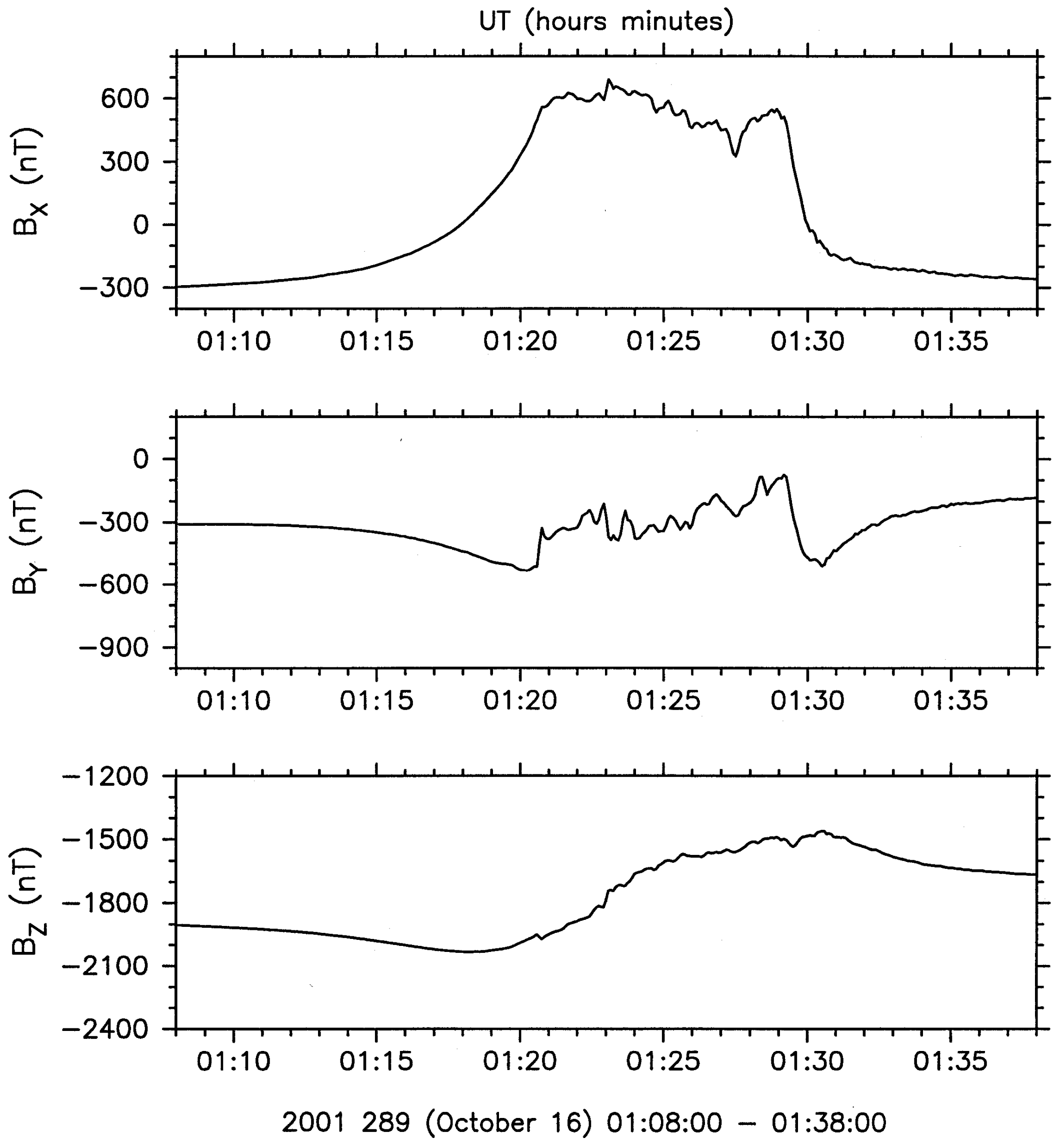
UT (hours minutes)
B_X (nT)
600
300
0
−300
01:10
01:15
01:20
01:25
01:30
01:35
B_Y (nT)
0
−300
−600
−900
B_Z (nT)
−1200
−1500
−1800
−2100
−2400
2001 289 (October 16) 01:08:00 – 01:38:00

Figure 6. Dependence of Jupiter's decametric radio emission on the position of Io (reproduced from Bigg (1964)).

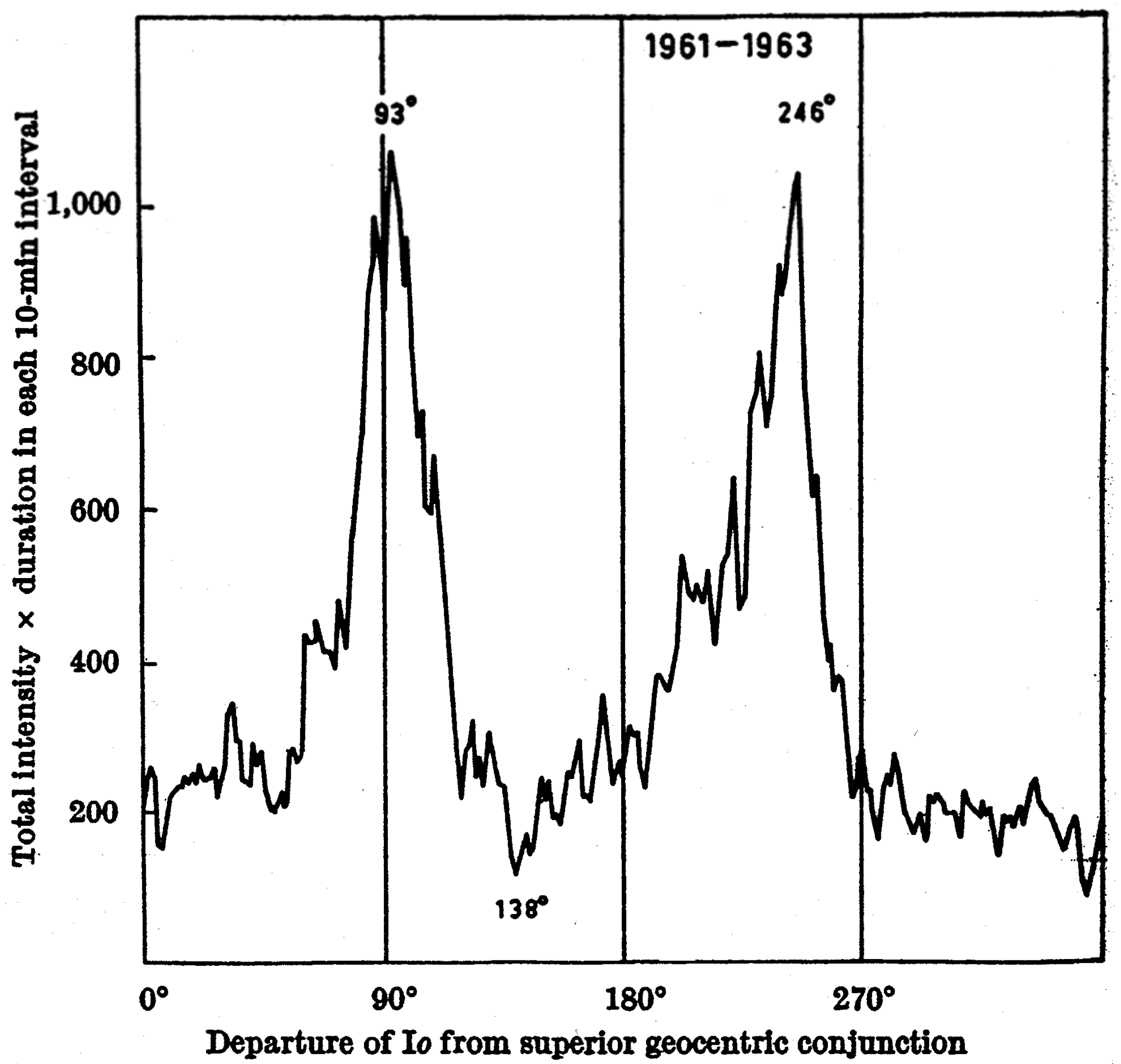

1961–1963
93°
246°
138°
1,000
800
600
400
200
0°
90°
180°
270°
Total intensity × duration in each 10-min interval
Departure of Io from superior geocentric conjunction

Figure 7. Meridian plane view of the current circuit of Io and Jupiter. Also, the trajectory of Galileo is shown (not to scale).

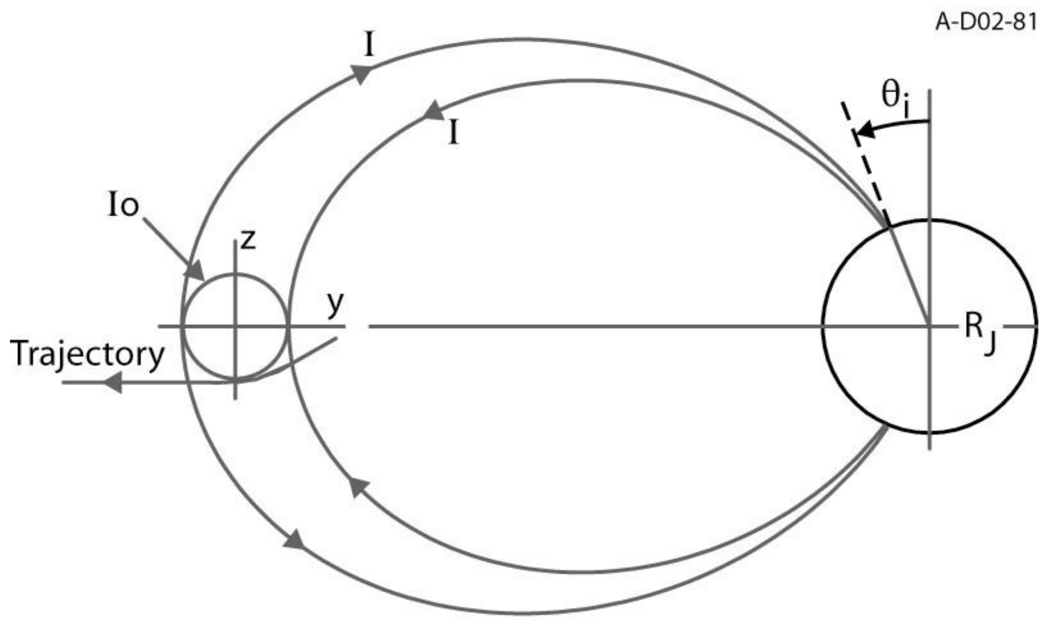
A-D02-81
I
I
θi
Io
z
y
Trajectory
RJ

Figure 8. Polar view of the current circuit of Io and Jupiter. Also, the trajectory of Galileo is shown (not to scale).

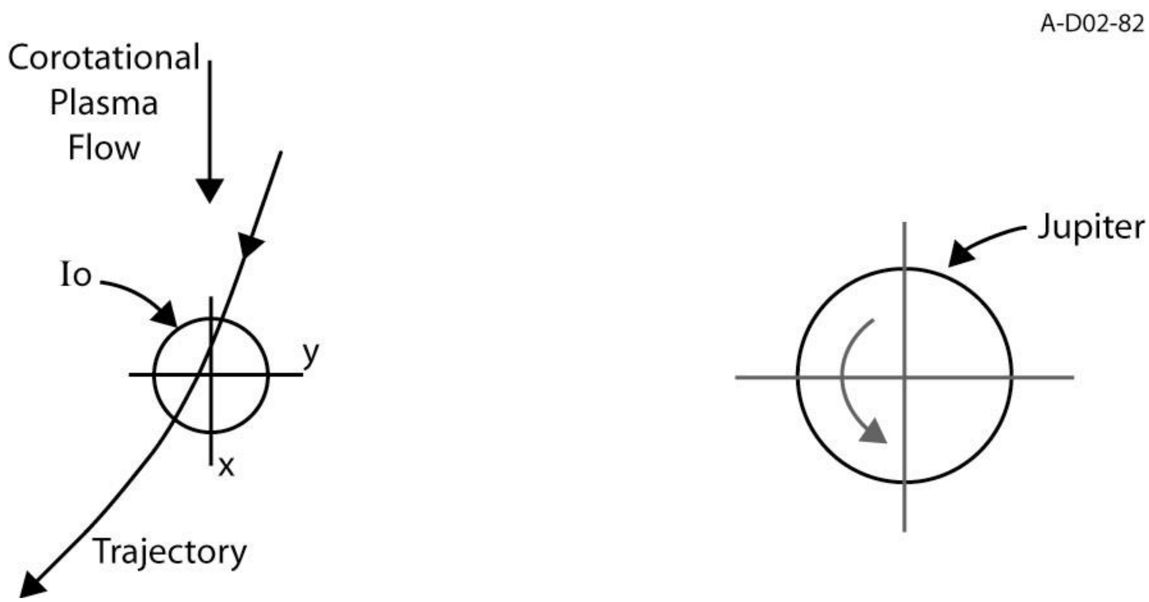
A-D02-82
Corotational
Plasma
Flow
Io
y
x
Trajectory
Jupiter

Figure 9. Left: Comparison of the observed perturbation magnetic field components and best-fit magnetic fields for twin oppositely directed currents and for a line current. Right: The magnetic field perturbation produced by the dipole source (reprinted from Ness *et al*. (1979)).

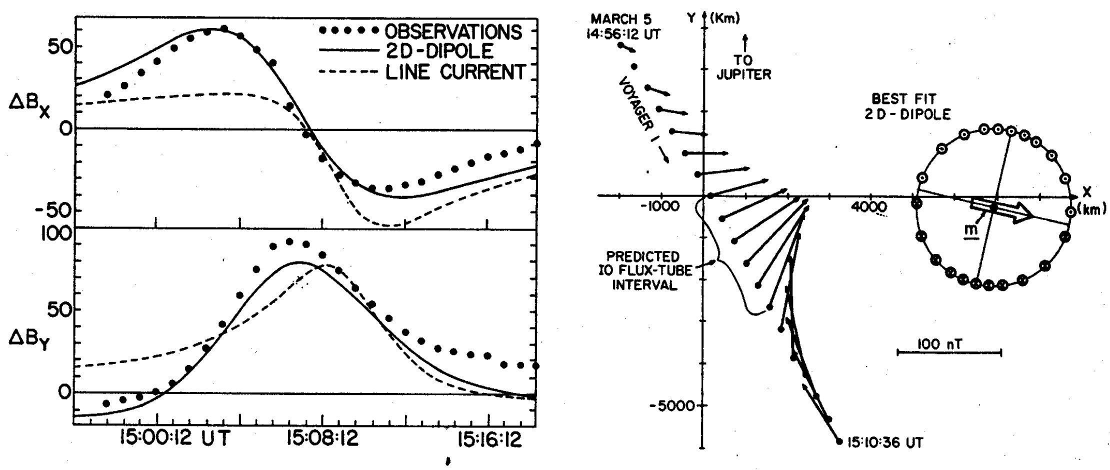
OBSERVATIONS
2D-DIPOLE
LINE CURRENT
ΔB_X
50
0
-50
100
50
ΔB_Y
0
15:00:12 UT
15:08:12
15:16:12
MARCH 5
14:56:12 UT
Y (Km)
TO
JUPITER
VOYAGER 1
BEST FIT
2D - DIPOLE
X
(km)
-1000
4000
m
PREDICTED
IO FLUX-TUBE
INTERVAL
100 nT
-5000
15:10:36 UT

Figure 10. Three-dimensional sketch of ‘Alfven wings’ generated by an ideal conductor in a collisionless plasma (after Drell (1965)).

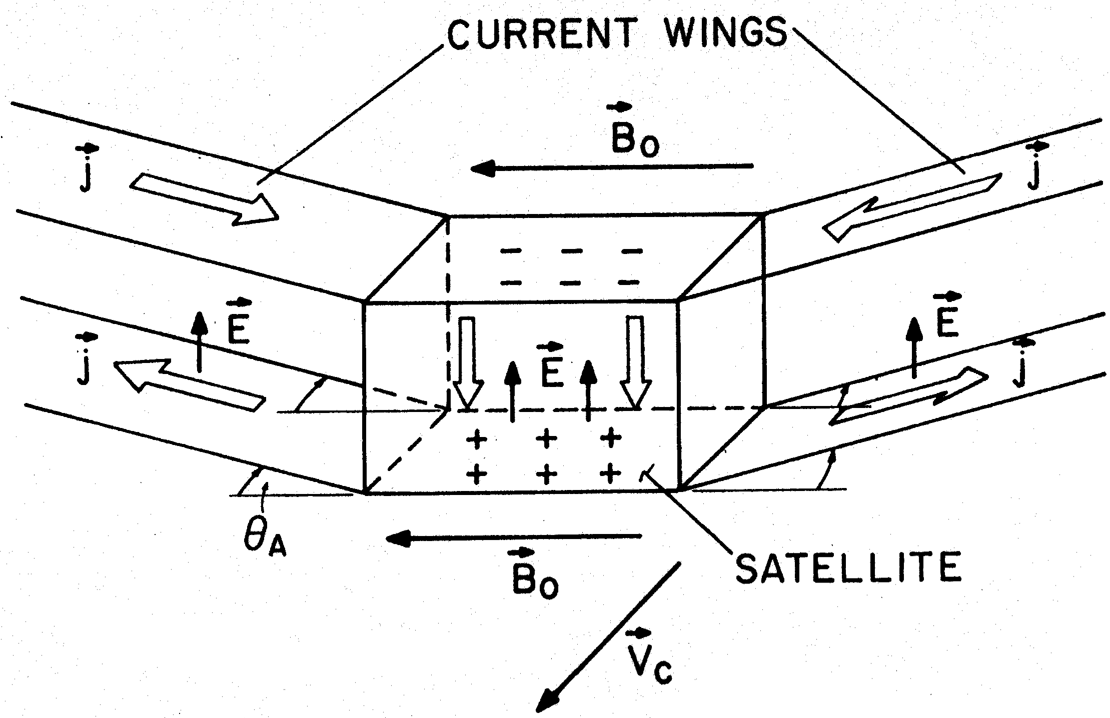
CURRENT WINGS
$\vec{B}_0$
$\vec{j}$
$\vec{j}$
$\vec{E}$
$\vec{j}$
$\vec{E}$
$\vec{E}$
$\vec{j}$
θ_A
$\vec{B}_0$
SATELLITE
$\vec{V}_c$

Figure 11. Polar plots of the surface of the index of refraction with frequencies f_1, f_2 and f_3. ($\theta_{\mathrm{Re}s}$ is the resonance cone angle when the index of refraction $n(\theta)$ goes to infinity. ψ the angle between limiting ray path direction and the magnetic field).

A-D02-104a

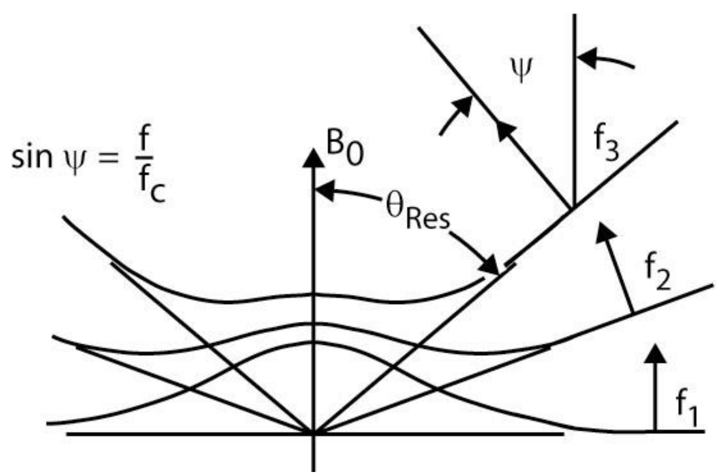

Figure 12. Demonstrating the propagation of whistler-mode waves from a point source.

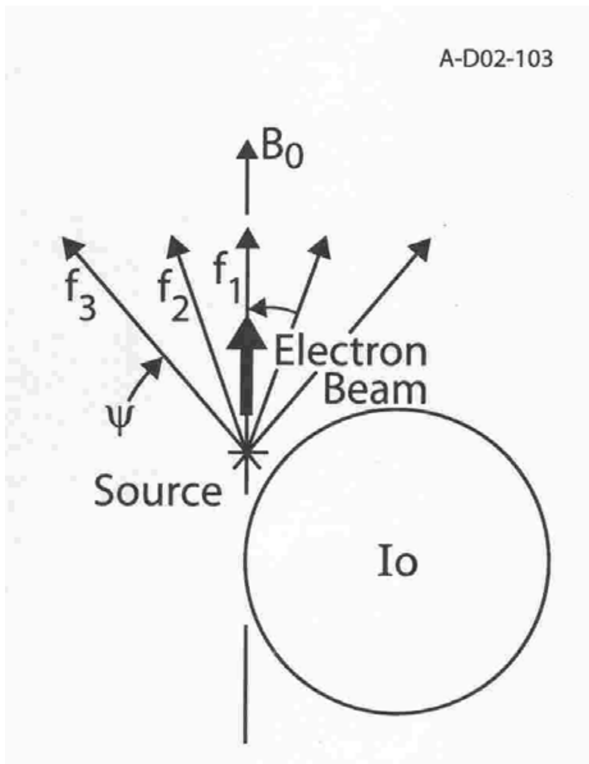
A-D02-103
B_0
f_3
f_2
f_1
Electron
Beam
ψ
Source
Io

Figure 13. Demonstrating the geometry of the produce of a funnel-shaped low frequency cutoff.

A-D03-64

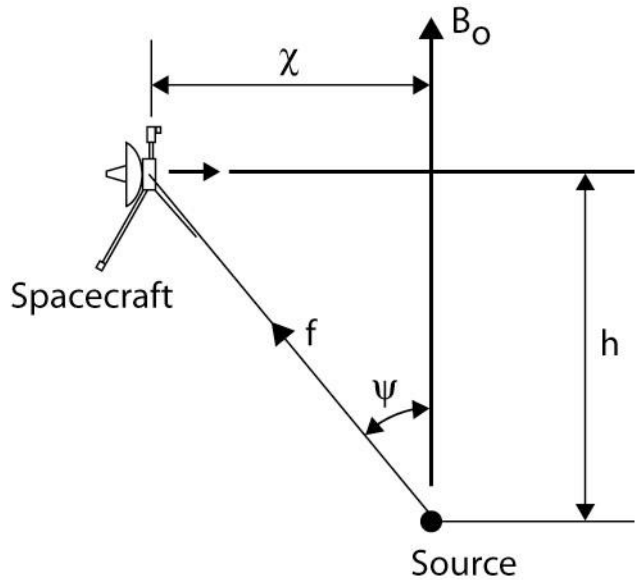

Figure 14. Funnel-shaped low frequency cutoff calculated from whistler-mode propagation near resonance cone.

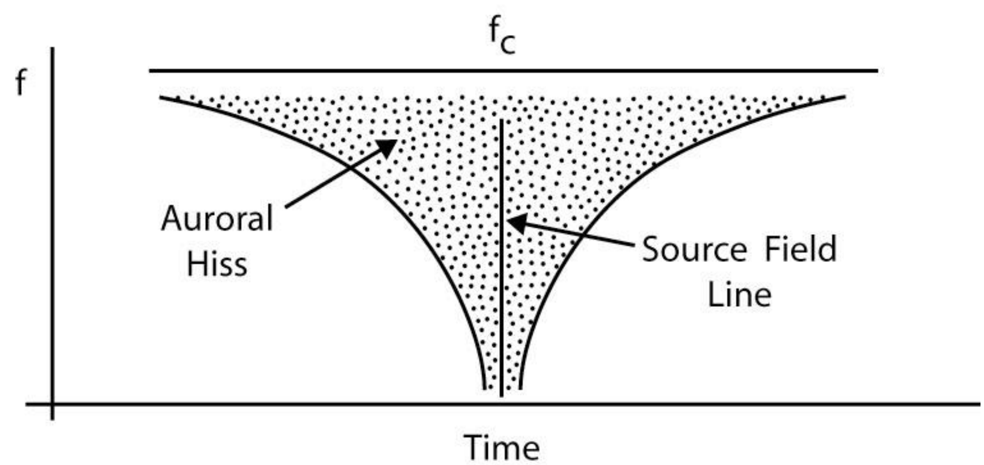
f
f_c
Auroral
Hiss
Source Field
Line
Time

Figure 15. Demonstrating the geometric relation for locating the point source position when using best-fit propagation cutoff.

A-D02-96

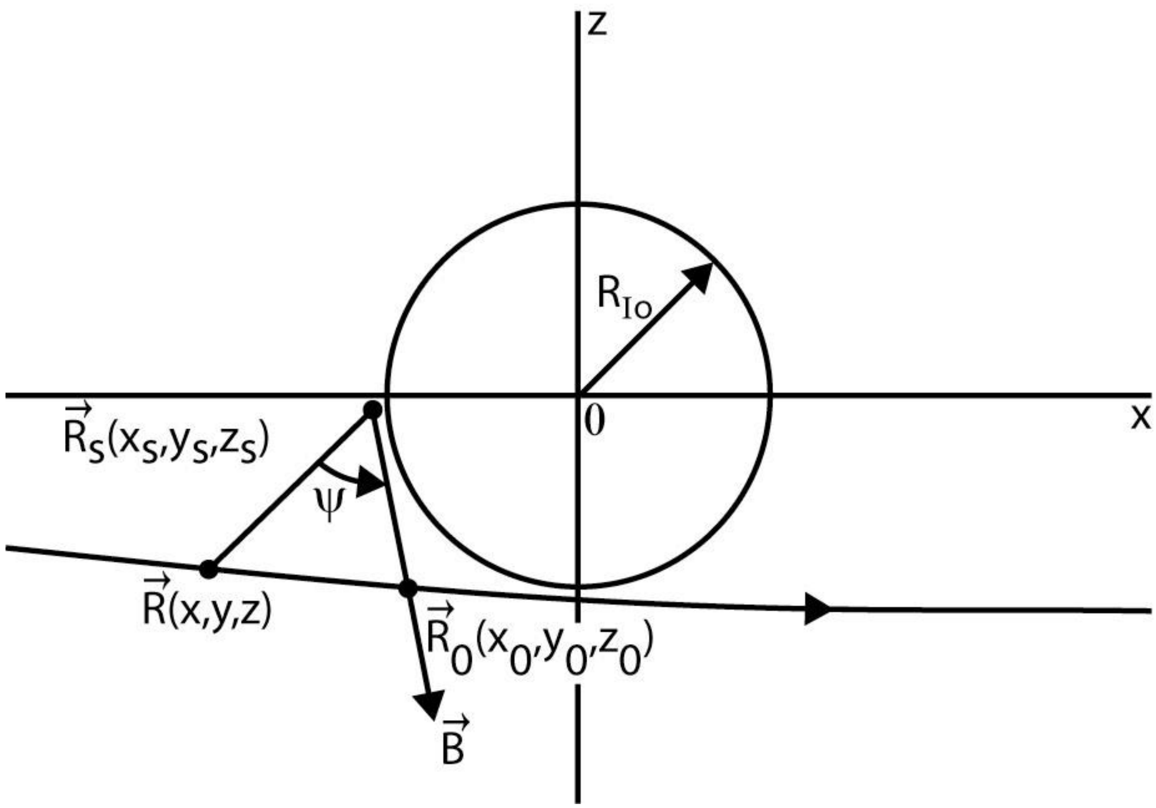

Figure 16. Fitting curves for three different point source positions. (The solid circles are sampled from the cutoff emission boundary of the spectrum; three fitting curves are calculated for three different source positions.)

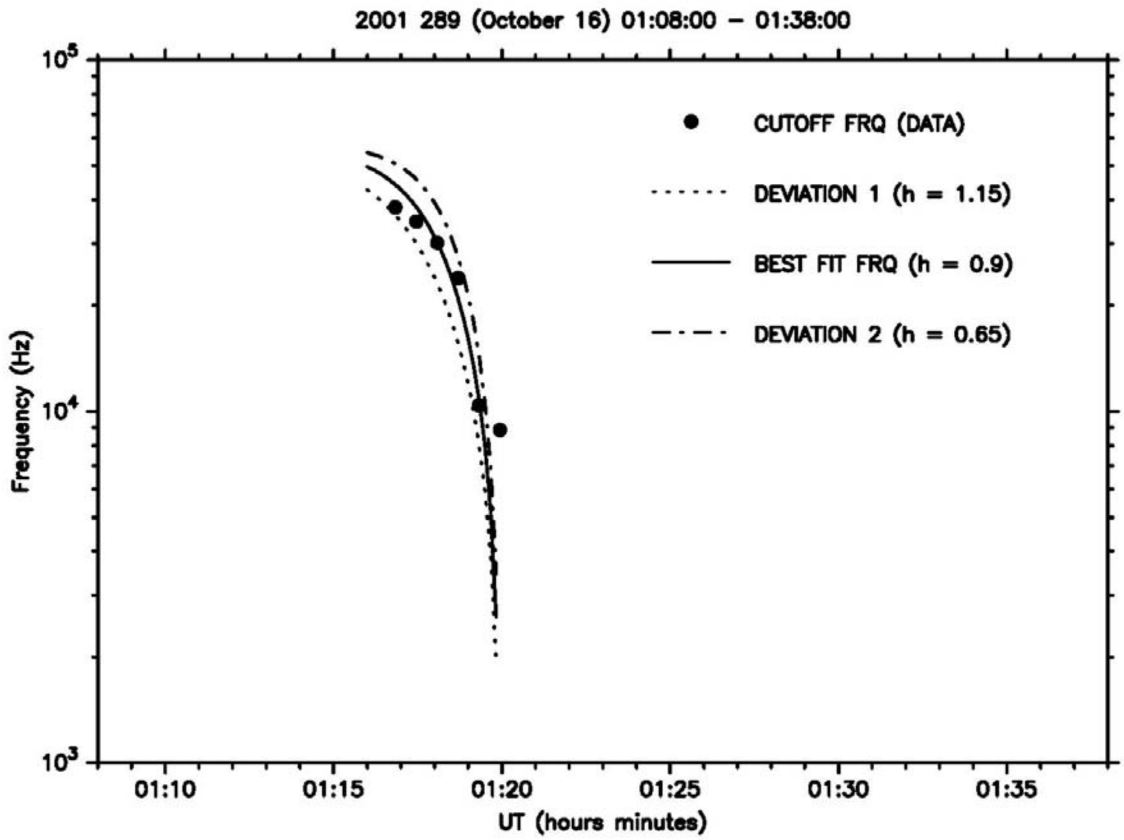
2001 289 (October 16) 01:08:00 – 01:38:00
CUTOFF FRQ (DATA)
DEVIATION 1 (h = 1.15)
BEST FIT FRQ (h = 0.9)
DEVIATION 2 (h = 0.65)
Frequency (Hz)
UT (hours minutes)
01:10
01:15
01:20
01:25
01:30
01:35

Figure 17. The best-fit curve for a point source is plotted on the spectrum.

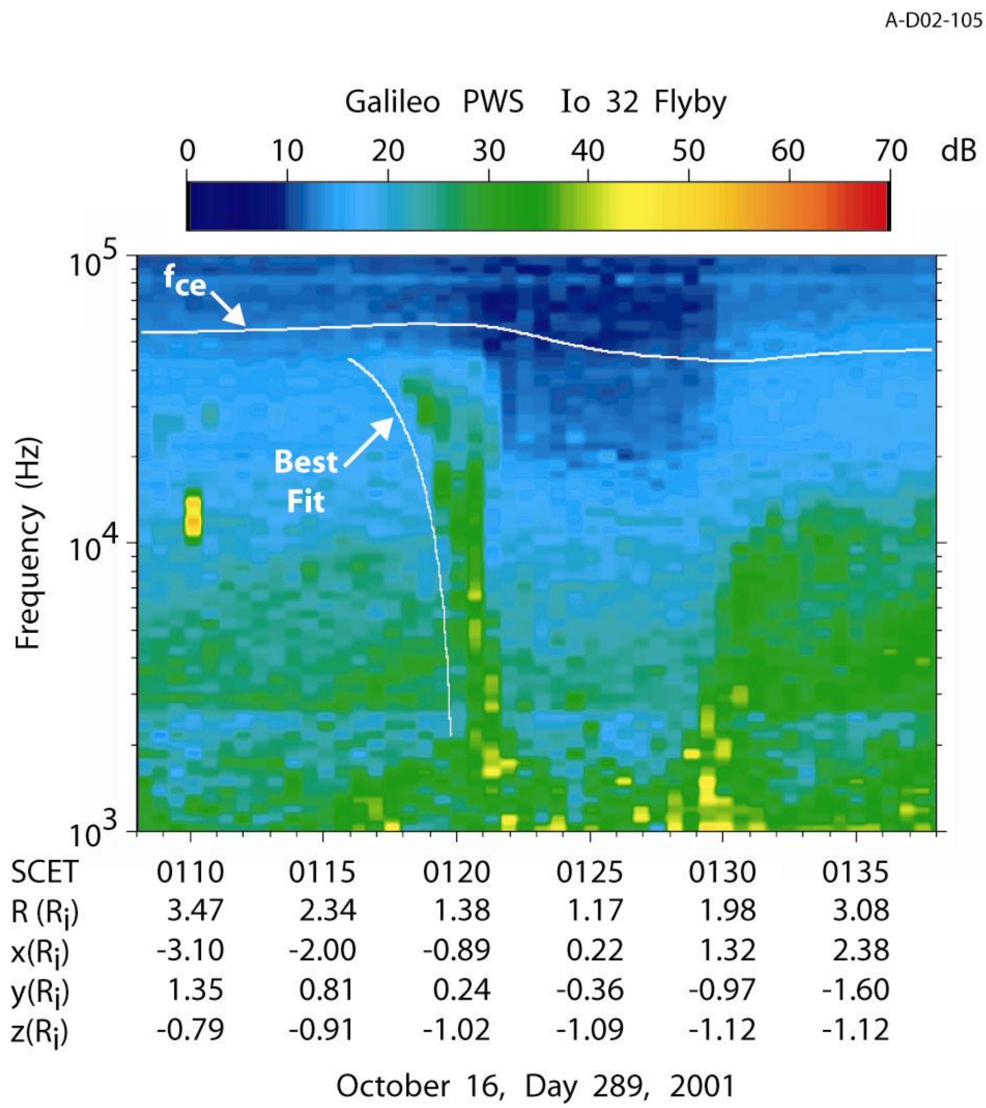
A-D02-105
Galileo PWS Io 32 Flyby
0
10
20
30
40
50
60
70
dB
10^5
f_{ce}
Best Fit
10^4
Frequency (Hz)
10^3
SCET
0110
0115
0120
0125
0130
0135
R (R_i)
3.47
2.34
1.38
1.17
1.98
3.08
x(R_i)
-3.10
-2.00
-0.89
0.22
1.32
2.38
y(R_i)
1.35
0.81
0.24
-0.36
-0.97
-1.60
z(R_i)
-0.79
-0.91
-1.02
-1.09
-1.12
-1.12
October 16, Day 289, 2001

Figure 18. A three-dimensional plot showing the geometric calculation for a sheet emission source.

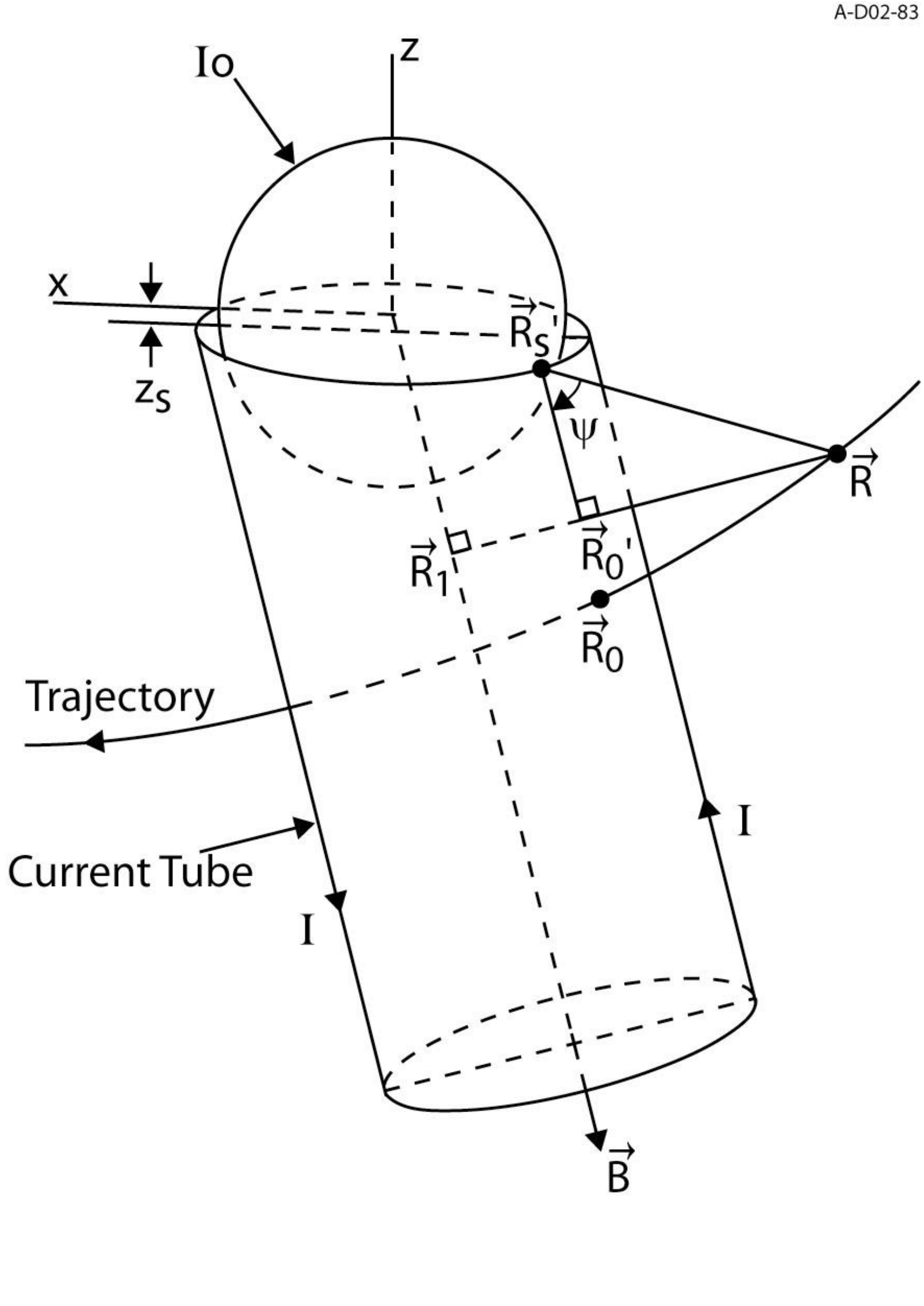
A-D02-83
z
Io
x
z_S
$\vec{R}_S$'
ψ
$\vec{R}$
$\vec{R}_1$
$\vec{R}_0$'
$\vec{R}_0$
Trajectory
Current Tube
I
I
$\vec{B}$

Figure 19. Cutoff frequency calculated from a sheet emission source (solid line) versus the sampled cutoff data (solid circles).

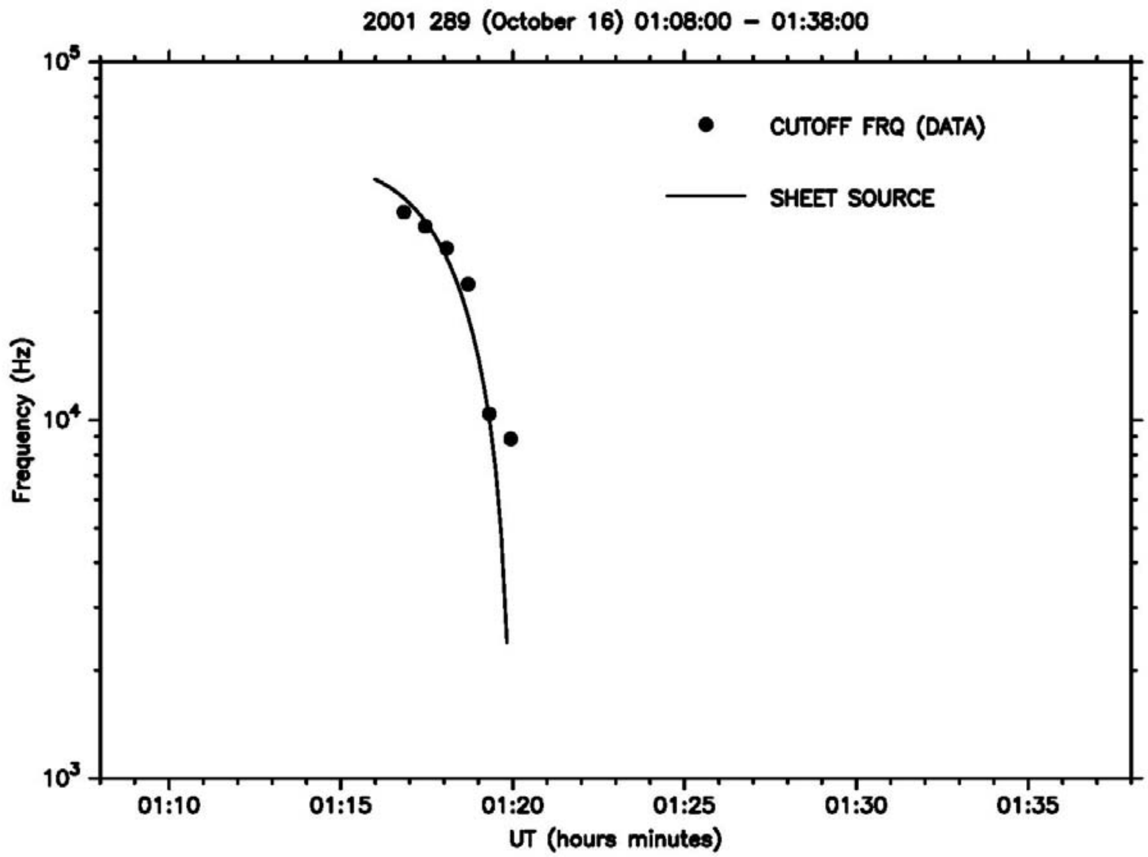
2001 289 (October 16) 01:08:00 – 01:38:00
CUTOFF FRQ (DATA)
SHEET SOURCE
Frequency (Hz)
UT (hours minutes)
01:10
01:15
01:20
01:25
01:30
01:35

REFERENCES

Bigg, E.K., Influence of the satellite Io on Jupiter's decametric emission, *Nature*, **203**, 1008, 1964.

Burke, B.F. and K.L. Franklin, Observations of a variable radio source associated with the planet Jupiter, *J. Geophys. Res*., **60**, 213-217, 1955.

Carr, T.D., M.D. Desch and J.K. Alexander, Phenomenology of magnetospheric radio emissions, *Physics of the Jovian Magnetosphere*, ed. A.J. Dessler, Cambridge University Press, London, 1983.

Fran Bagenal, Empirical model of the Io plasma torus: Voyager measurements, *J. Geophys. Res.*, **99**, 11043-11062, 1994.

Farrell, W.M. and D.A. Gurnett, An analysis of whistler-mode radiation from the Spacelab 2 electron beam, *J. Geophys. Res.*, **93**, 153-161, 1988.

Goldreich, P., and Donald Lynden-Bell, Io, a Jovian unipolar inductor, *Astrophys. J.*, **156**, 59, 1969.

Gurnett, D.A., High-latitude geophysical studies with satellite Injun 3, *J. Geophys. Res.*, **69**, 65-89, 1964.

Gurnett, D.A., A Satellite study of VLF hiss, *J. Geophys. Res.*, **71**, 5599-5615, 1966.

Gurnett, D.A., Sheath effects and related charged-particle acceleration by Jupiter's satellite Io, *Astrophys. J.*, **175**, 525-533, 1972.

Gurnett, D.A. and A. Bhattacharjee, *Introduction to Plasma Physics with Space and Laboratory Applications*, Cambridge University Press, in press, 2003.

Gurnett, D.A. and L.A. Frank, VLF hiss and related plasma observations in the polar magnetosphere, *J. Geophys. Res.*, **77**, 172, 1972.

Gurnett, D.A., and W.S. Kurth, Auroral hiss observed near the Io plasma torus, *Nature*, **280**, 767, 1979.

Gurnett, D.A. and B.J. O'Brien, High-latitude geophysical studies with satellite Injun 3, *J. Geophys. Res.*, **69**, 65-89, 1972.

Gurnett, D.A., S.D. Shawhan, and R.R. Shaw, Auroral hiss, Z mode radiation, and auroral kilometric radiation in the polar magnetosphere: DE 1 observations, *J. Geophys. Res*., **88**, 329-340, 1983.

Gurnett, D.A., W.S. Kurth, A. Roux, S.J. Bolton, E.A. Thomsen, and J.B. Groene, Galileo plasma wave observations near Europa, *J. Geophys. Res*., **25**, 237-240, 1998.

Gurnett, D.A., W.S. Kurth, R.R. Shaw, A. Roux, R. Gendrin, C.F. Kennel, F.L. Scarf, and S.D. Shawhan, The Galileo plasma wave investigation, *Space Sci. Rev*., **60**, 341-355, 1992.

Kivelson, M.G., K.K. Khurana, J.D. Means, C.T. Russell and R.C. Snare, *Space Sci. Rev.*, **60**, 357(1992).

Kliore, A., D.L. Cain, G. Fjeldbo, B.L. Seidel, S.I. Rasool, Preliminary results on the atmospheres of Io and Jupiter from Pioneer 10 S-Band occultation experiment, *Science*, **183**, 323-324, 1974.

Martin, L.H., R.A. Helliwell, and K.R. Marks, Association between aurorae and very-low-frequency hiss observed at Byrd Station, Antarctica, *Nature*, **187**, 751-753, 1960.

Ness, N.F., M.H. Acuna, R.P. Lepping, L.F. Burlaga, K.W. Behannon, and F.M. Neubauer, Magnetic field studies at Jupiter by Voyager 1: Preliminary results, Science, 203, 42-46, 1979.

Neubauer, F.M., Nonlinear standing Alfven wave current system at Io: Theory, *J. Geophys. Res.,* **85**, 1171-1178, 1980.

Stix, T.H., *The Theory of Plasma Waves*, McGraw-Hill, New York, 1962.

Storey, L.R.O., An investigation of whistling atmospherics, *Phil. Trans. Roy. Soc. London, A*, **246**, 113-141, 1953.